Washington University in St. Louis

Comparison of Diffusion MRI with Axonal Trajectories Near Cortex to Estimate Folding-Related Biases of Tractography-based Connectivity in the Macaque Brain

Author:
Charlie Chen

Supervisor:
David Van Essen

A thesis submitted in fulfillment of the requirements for the degree of Bachelor of Arts in the

Department of Biology

May 2016

WASHINGTON UNIVERSITY IN ST. LOUIS

Abstract

David Van Essen
Department of Biology

Comparison of Diffusion MRI with Axonal Trajectories Near Cortex to Estimate Folding-Related Biases of Tractography-based Connectivity in the Macaque Brain

by Charlie Chen

Diffusion MRI and probabilistic tractography are powerful tools for analyzing long-distance connections within the white matter of the brain, but technical limitations of these methods have become increasingly apparent. One such limitation in current tractography algorithms results in a folding-related bias in apparent connectivity. In particular, there is a tendency for tractography streamlines to preferentially terminate at gyral crowns, compared to sulcal banks and fundi. This leads to folding-dependent discrepancies between the estimates of connectivity in diffusion data versus tracer and histology data. As tracer and histology data are considered to be closer to neuroanatomical ground truth, the origin for the gyral bias lies within the methods by which diffusion fiber orientations are modeled and how tractography streamlines are generated.

Here, the extent of this gyral bias was quantified through comparing diffusion MRI fiber orientations with ground truth neuroanatomy given by an analysis of axonal trajectories from histology. Comparisons made with a structure tensor modelling of histology fiber orientations were validated against manual orientation comparisons, and were used to expedite image analysis. Finally, non-linear registration of histology volumes generated by two-photon microscopy of tissue-cleared samples allows comparison of fiber orientation components in three-dimensions between diffusion MRI and histology. Such observations can potentially be expanded into a set of anatomical priors for use in informing diffusion modeling and tractography in white matter close to the cortical gray matter sheet.

Acknowledgements

Thanks to Dr. Van Essen and Dr. Dikranian for mentorship and guidance over the last three years. Thanks to Matt for putting up with me, and to the rest of Van Essen lab - Jenn, John H., John S., Donna, Erin, Chad, Nathan, and Tim. Thanks to Susan and everyone up in the departmental business office.

Thanks to Katherine Holzem and the Efimov lab for producing cleared and stained tissue samples. Thanks to Dr. Olney and his lab for their generosity in making postnatal macaque histology sections available for our use. Thanks to Dr. Price for sharing the Gallyas myelin-stained sections and Dr. Bridgman for technical advice. Thanks to Kris and Gary and the Hope Center Alafi Neuroimaging Lab for use of the Nanozoomer. Thanks to Mr. Oakley and the Bakewell NeuroImaging Laboratory for their extensive advice and use of the two-photon confocal.

Text is typeset in LaTeX modifying an earlier template made available by Steven Gunn and Sunil Patel under a CC BY-NC-SA 3.0 license.

Funded by NIH R01-MH-60974 (DVE); Human Connectome Project (1U54MH091657-01) from the 16 NIH Institutes and Centers that Support the NIH Blueprint for Neuroscience Research; NIH F30 MH097312 (MFG); HD052664 (JO) and grant HD 062171 (JO). We acknowledge support from the Hope Center Alafi Neuroimaging Lab, and a P30 Neuroscience Blueprint Interdisciplinary Center Core award to Washington University (P30 NS057105).

Contents

Chapter 1

Folding-related biases in MR diffusion tractography

1.1 Introduction

Diffusion MRI and probabilistic tractography are powerful tools for analyzing long-distance connections within the white matter of the brain. However, technical limitations of these connectomes have become increasingly apparent. One such limitation is the tendency for tractography streamlines to preferentially terminate at gyral crowns. Figure 1.1 shows the extent of this gyral bias with a streamline density map of a post-mortem macaque brain. The density map gives the count of the mean number of streamlines that reach each cortical vertex after seeding white matter voxels over the entire hemisphere. The figure shows high streamline density (red) at gyral crowns and low streamline density (indigo and black) at sulcal fundi, indicating a preference for tractography streamlines to terminate at gyral crowns.

This observation does not reflect the current understanding of anatomical inputs and outputs to cortex as revealed by modern tracer studies. Figure 1.2 shows selected results from the tracer study performed in Markov *et al.* (2012) [2]. Among other observations, cortico-cortical connections between any two given areas are organized in an irregular pattern that does not demonstrate preferential termination at either gyral crowns or sulcal fundi.

As the gyral bias is not accounted for by neuroanatomical ground truth, its origins must lie in how diffusion data is acquired and how tractography streamlines are generated. In tractography, current algorithms propagate streamlines by selecting the fiber with the least deviation from the current streamline direction. In deep white matter, this

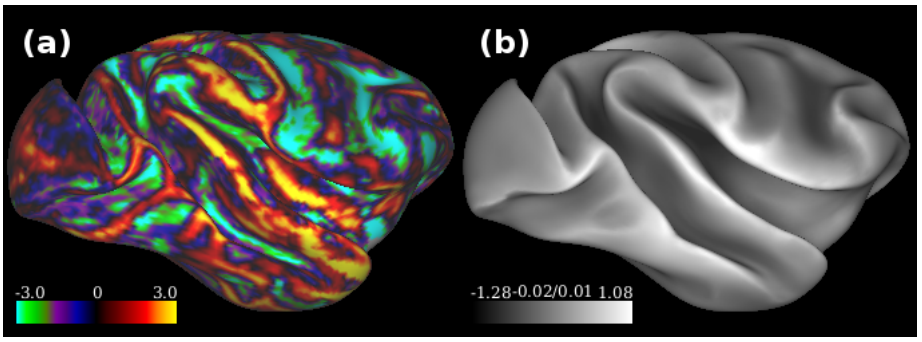

FIGURE 1.1: Gyral bias in probabilistic tractography. (a) A streamline density map of the right hemisphere of a postmortem macaque brain. The figure is colored with respect to the mean number of streamlines that reach each cortical vertex, with red indicating a high number of streamlines and indigo and black indicating a low number of streamlines. (b) A FreeSurfer 'sulc' map reveals gyri as brightly colored areas and sulci as darker areas. Comparing the two maps, it is apparent that gyral crowns consistently have higher streamline counts than sulcal fundi, suggesting a gyral bias in the tractography. Adapted from Van Essen *et al.* (2014) [1].

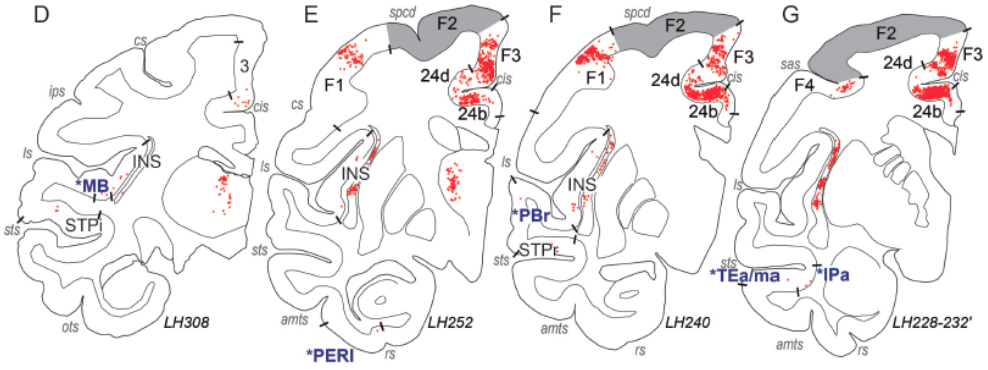

FIGURE 1.2: Connectivity bias absent in tracer studies. Drawings of coronal sections after single retrograde tracer injection in area F2 in the motor cortex show irregular pattern of connectivity. Injection site is starred red, injected area F2 is shaded gray, labeled neurons are shown as red dots. No noteworthy bias in cortical termination sites is found among the labeled neurons. Adapted from Markov *et al.* (2012) [2].

assumption of streamline continuity allow tractography algorithms to follow tightly-bundled fiber tracts. However, when entering a cortical gyrus, the current streamline direction typically points to the crown of the gyrus, and the standard tractography algorithms assume maximal streamline continuity, this precludes streamlines from taking the sharper angles needed to terminate at gyral banks and sulcal fundi.

Furthermore, in the diffusion data itself, radial fibers normal to the cortical surface are absent or show weak signal near gyral banks and sulcal fundi. This is best shown in Figure 1.4. For each cortical vertex, the dot product between the fiber orientations in the white matter voxel nearest to the surface and the surface normal was taken. Fibers orientations that approximate the surface normal seem to locate at gyral crowns. However, the absence of these small angle fibers along gyral banks and sulcal fundi

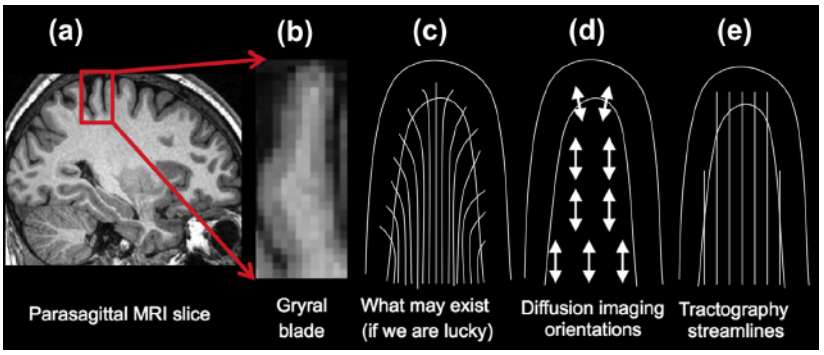

FIGURE 1.3: Assumptions of tractography which contribute to a gyral bias. (a) A parasagittal MRI slice. (b) A cortical gyrus. (c) Possible underlying neuroanatomical structure of axonal terminations. Fibers terminate without preference to cortical location, though fibers terminating at the gyral bank will take sharper angles to do so. (d) Fiber orientations from diffusion imaging. The orientations point predominantly towards the crown. (e) Tractography streamlines select fibers that minimize angular deviation from the current direction and preferentially terminate at the gyral crown. Adapted from Van Essen *et al.* (2014) [1].

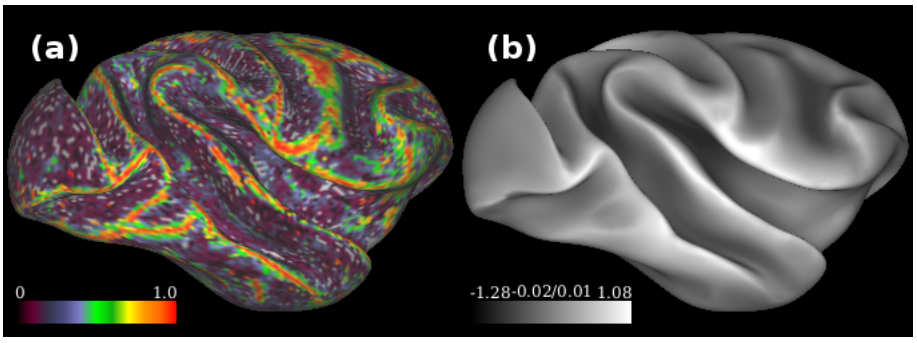

FIGURE 1.4: Few fibers approximate the surface normal outside of gyral crowns. (a) A FreeSurfer 'sulc' map shows how far each vertex point is located from a mid-surface computed between gyri, which lie above this surface, and sulci, which lie below. Vertices above the mid-surface are white and vertices below are black. (b) The dot product was taken between the fiber orientations in the white matter voxel nearest to the surface and the surface normal at each cortical vertex. The map shows fibers parallel to the surface normal in red, and fibers tangential to the surface normal in blue. Comparing both plots reveals that fibers pointing parallel to the surface normal are localized to gyral crowns. Adapted from Van Essen *et al.* (2014) [1].

indicate that tractography algorithms have little evidence from the diffusion data to support crossing of the gray/white boundary in these regions.

Chapter 2

Comparing diffusion MRI with 2D histology

2.1 Comparisons within a gyral blade

To eventually compensate for gyral bias in diffusion imaging, a validation approach was developed using myelin-stained histological sections of macaque cortex to compare against predictions from model-based analysis of diffusion-weighted MRI scans in macaque. The resolution of scanned histology sections is much higher than the resolution of diffusion data at equivalent levels, providing ground truth data in regions of low diffusion signal. Furthermore, histology data can reveal fiber orientation information that cannot be found using tracer data, to be used in validating diffusion orientation predictions. Histology preparation and diffusion MRI acquisition are described below.

During histology preparation, an adult macaque brain was perfusion-fixed with 4% paraformaldehyde, postfixed for 24 hours at 4°C, and sectioned coronally at 70 µm intervals by vibratome. The floating sections were immunostained with antibody to myelin basic protein at 1:100 dilution, using VIP as the chromogen (MBP, MAB395, Millipore; Vactastain, Vector). After mounting, dehydration, and coverslipping, sections were scanned on a scanning microscope at 9.225 µm resolution (Nanozoomer, Hamamatsu). A Gallyas myelin-stained section of another adult macaque was similarly digitized.

During diffusion MRI acquisition, a diffusion-weighted MRI dataset of a perfusion-fixed adult macaque brain was acquired with a 4.7 T Bruker scanner. Scans used a 3D multi-shot spin-echo sequence, with an isotropic resolution of 430 µm [3] [4]. The ball and

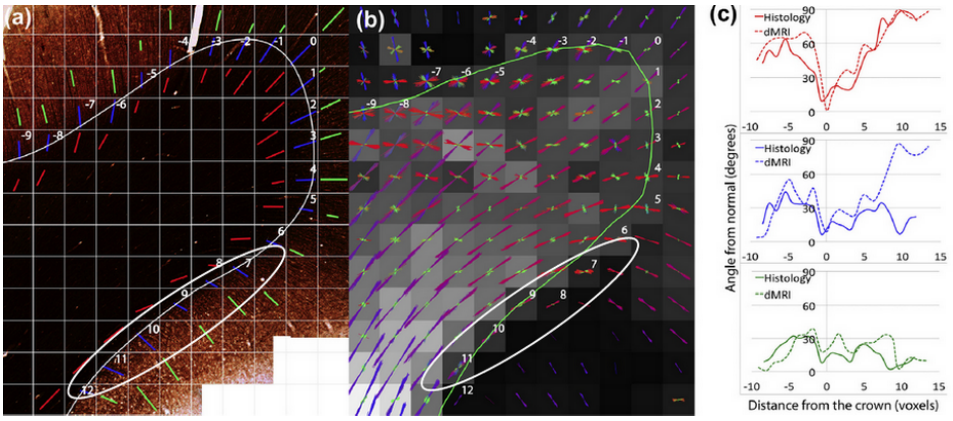

FIGURE 2.1: Comparing fiber orientations in histology and diffusion MRI near the gray/white boundary of a gyral crown. (a) On the Gallyas myelin-stained section, fiber orientations and gray/white boundary were drawn in Adobe Illustrator. Angle measures were sampled every 0.43 mm to approximate MRI voxel dimensions. (b) Diffusion imaging results from a different post-mortem macaque brain using the ball-and-stick model in FSL bedpostx to obtain estimates of the main fiber orientations for each voxel and visualized in Caret. Conventional color-coding is used to show components oriented medial-lateral (red), dorso-ventral (blue), and antero-posterior (green). The gray/white boundary (green surface) was generated by a thresholded sum of anisotropy image and edited in Caret. (c) A cross-modal comparison of fiber orientation in subcortical white matter (red), at the gray/white boundary (blue), and in deep-layer cortex (green). Angles are reported clockwise, in degrees relative to the local surface normal.

stick model was fitted to the data to estimate main fiber orientation in each imaging voxel [5].

Our analysis was restricted to the superior frontal gyrus of the left hemisphere of both macaques. This region includes many unbroken radial fibers, which indicate that the section was cut near-orthogonal to the radial axis and can be compared to MRI sections of an equivalent region. Main fiber orientations were compared in the histology and diffusion-weighted MRI. First, a path defining the gray/white matter boundary was manually delineated in Adobe Illustrator. Points were selected along the boundary at intervals of 0.43 mm to approximate the dimensions of an MRI voxel. At each point, the angle of the main fiber orientation against the local surface normal of the gray/white boundary was obtained when the fiber is within subcortical white matter (red), as it passes the gray/white boundary (blue) and as it enters cortex (green). These angles were plotted as a function of distance from the gyral crown. Distances between histology and diffusion MRI were aligned by locating corresponding anatomical landmarks in both sections and normalizing the distances between the landmarks.

From Figure 2.1, there is good agreement between angle measures in histology (solid lines in graph) and diffusion MRI (dashed lines in graph) along the superior bank and gyral crown. However, discrepancies arise along the inferior bank leading towards the gyral sulcus (circled in white). Although diffusion fiber orientations in many regions are

validated by histology, orientations in regions of low total anisotropy, as indicated by the darker voxels, are highly inaccurate. To determine the consistency of these results, additional regions of interest were selected.

2.2 Comparisons across sections

The process of finding fiber orientations was improved to run semi-automatically over entire histology sections. In MATLAB, selected points along the gray/white boundary were used as control points to generate a spline function to delineate the gray/white boundary. Structure tensor analysis was performed to compute fiber orientations in a square region enclosing each control point, with dimensions to approximate a MRI voxel [6] [7]. Fiber orientations within each region were regrouped to generate mean fiber orientations and measured against the normal vector of the gray/white boundary at each control point as defined by the spline function. Distances were measured from the first control point laid, which was chosen to coincide with an anatomical landmark (the cingulate sulcus).

Angle measures in diffusion MRI were obtained using operations in Workbench Command. Angles to correspond to subcortical white matter, gray/white boundary, and deep-layer cortex angle measures in the histology were obtained by first generating new surfaces a small distance above and below the white surface to correspond to deep-layer cortex and subcortical white matter. This is implemented such that between a new surface and the white surface is enclosed a volume 10% of the total volume between the pial and the white surface. The white surface itself serves as the gray/white boundary. Along each surface, at vertices approximating the contour delineated in the histology, the dot product of the surface normal and the mean direction of each fiber population is taken and converted into an angle measure. For distance measures, each surface is used to generate a metric that gives the geodesic distance computed from the vertex closest to the anatomic landmark in the histology to all other vertices.

Across sections, histology and diffusion MRI show reasonable agreement, especially in white matter and near gyral crowns. Discrepancies occur where the structure tensor analysis correctly determines the sharp angles of terminating fibers, compared to diffusion MRI, which shows fibers running near tangential to the surface at several gyri. Other errors involve aligning a fundamentally two-dimensional histology with three-dimensional MRI using normalized geodesic distances measured from one anatomical landmark. Efforts to improve registration between the two surfaces might reduce errors resulting from misalignment. But where there are similarities between histology and MRI, orientation estimates of MRI are validated.

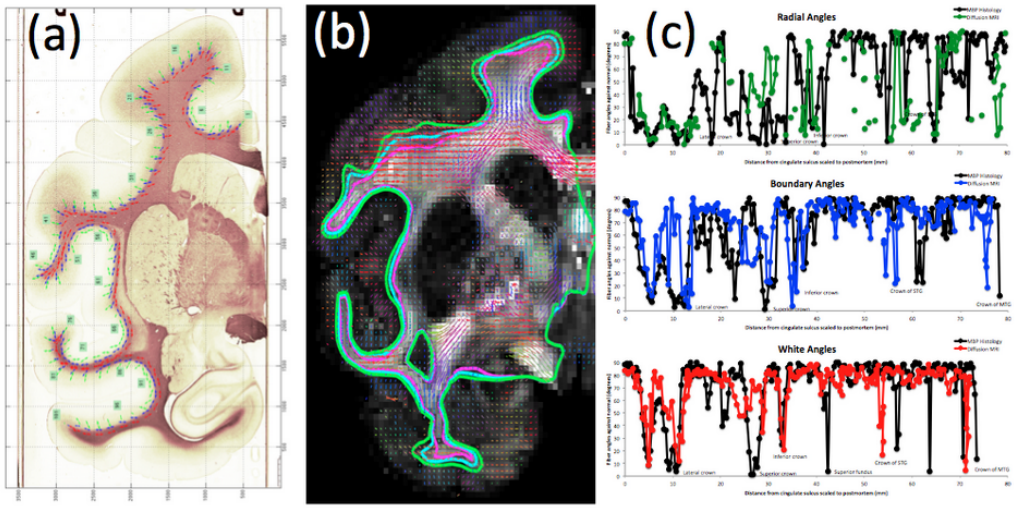

FIGURE 2.2: Comparing fiber orientations near the gray/white boundary across the coronal section of an adult macaque. (a) On the immunostained section, fiber orientations and gray/white boundary were generated in MATLAB. (b) Diffusion orientations were generated from FSL bedpostx and the gray/white boundary was generated by a thresholded sum of anisotropy image. Fiber orientations were visualized in Connectome Workbench. The subcortical white surface is shown in red, gray/white surface in blue, and deep-layer cortex surface in green. (c) A cross-modal comparison with orientations in subcortical white matter in red, gray/white boundary in blue, and deep-layer cortex in green.

Chapter 3

Comparing diffusion MRI with 3D histology

3.1 Image acquisition

More recently, an attempt was made to image three-dimensional tissue sections, as these can provide better validation of three-dimensional MRI data than two-dimensional sections, which cannot resolve out-of-plane fiber directions. During histology preparation, an adult macaque brain was perfusion-fixed with 4% paraformaldehyde, postfixed for 24 hours at 4 , and, sectioned coronally at 500 µm intervals by vibratome. The floating sections were cleared using the CLARITY protocol [8], except that no electrophoresis was performed. Instead, sections were cleared in static clearing buffer to allow for a gentler clearing process to minimize tears in tissue.

After clearing, sections were incubated with antibody to myelin basic protein at 1:50 dilution for 5 days, rinsed for an additional day, and incubated with secondary antibody at 1:100 dilution for 2 days, with a final day for rinsing. The secondary antibody is tagged with a far-red fluorescent probe for imaging, which avoids autofluorescent signal in brain tissue (Alexa Fluor 633, Molecular Probes).

After staining, sections were incubated in a clearing solution for 2 weeks to increase the transparency of the samples before imaging (FocusClear, Cedarlane Labs). Sections were then transferred to tissue culture grade polystyrene glass bottom Petri dishes, which provide high effective numerical aperture during high-resolution microscopy (GWSB-5040, WillCo Wells). Microscopy images were acquired on a two-photon confocal microscope at isotropic 0.003920 mm resolution (LSM-510 NLO 2-Photon/Confocal, Zeiss). A 15.27 mm $\times$ 15.27 mm overview image of the region of interest was acquired. Z-stacks of the

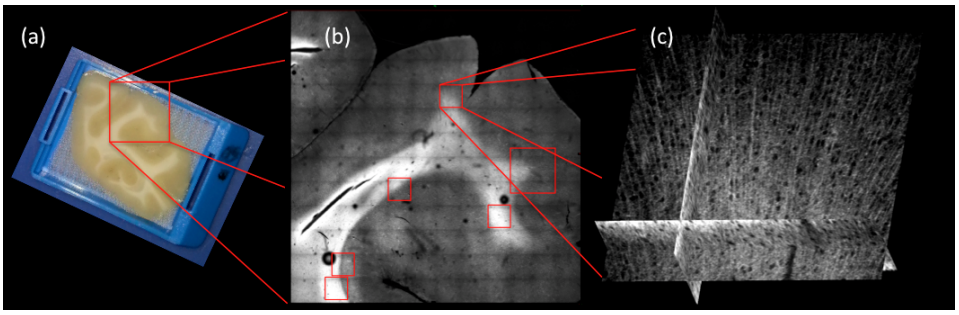

FIGURE 3.1: Image acquisition from the histology. (a) A 500 µm thick coronal histology section. Section was cleared via CLARITY protocol and labeled with fluorescent probe during immunohistochemistry. (b) Microscopy image of a 15.27 mm × 15.27 mm region of interest on stained section was acquired with a two-photon confocal microscope. Z-stacks of the crowns, bank, and sulcal fundus were then acquired (red boxes). (c) A z-stack of one of the crowns, measuring 1.16 mm × 1.16 mm × 0.42 mm.

crowns, banks, and sulcal fundus were then acquired, with depths approximating the thickness of a MRI voxel.

3.2 Image registration

Using positional information recorded during microscopy, the z-stacks were placed into a histology domain with the 15.27 mm × 15.27 mm overview image serving as a reference. The overview image was processed for registration by extracting the cortical ribbon in MATLAB using a spline function. A cortical ribbon from the same region of interest in the MRI was also extracted, using signed distance functions available in the command-line options in Connectome Workbench (http://www.humanconnectome.org/software/connectome-workbench.html) with the white and pial surfaces as serving as the boundaries. The cortical ribbon generated from the microscopy was then registered in elastix software (http://elastix.isi.uu.nl/) to the cortical ribbon generated from the MRI with a non-rigid transformation using B-splines as the parametrization. The resulting transform was stored as a deformation field.

3.3 Fiber visualization

The deformation field computed from the registration was used to resample all z-stack volumes from the microscopy into the MRI domain. Z-stack volumes were resampled into volume spaces and regrouped into voxels one-eighth the volume of a MRI voxel. Resampled volumes were correctly oriented in relation to the corresponding region in the MRI. Volumes were processed by voxelwise structure tensor analysis, and these

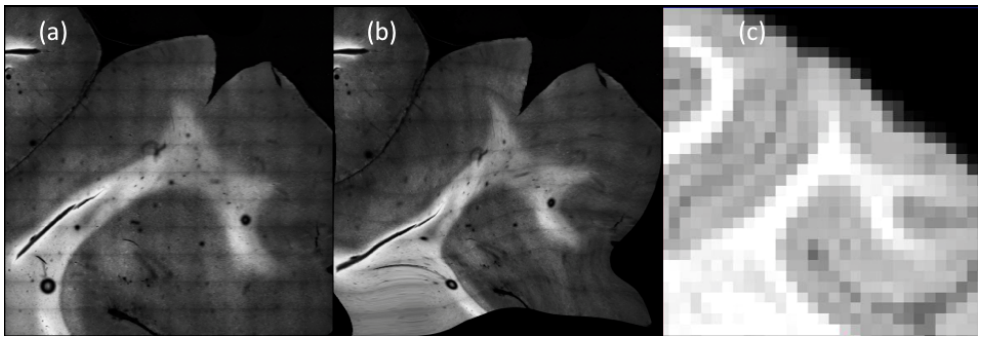

FIGURE 3.2: Image registration with the histology. (a) The previous microscopy image of the region of interest. (b) The image after registration to an equivalent region in the MRI. (c) The region of interest as found in a T1-weighted scan of a postmortem macaque.

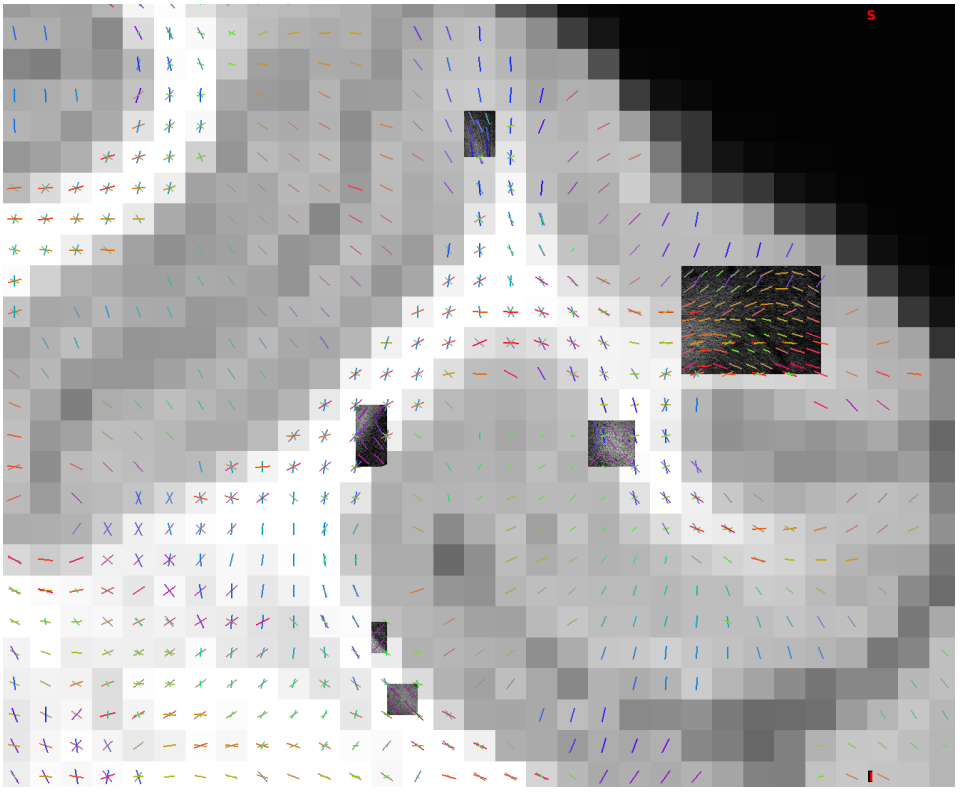

FIGURE 3.3: Histology z-stacks resampled into appropriate volume spaces with voxel volumes that are one-quarter the volume of a MRI voxel. Histology fibers were generated with voxelwise structure tensor and converted to bingham distributions to display (shown without fanning estimates). Diffusion MRI fiber estimates were generated using rubiX estimates with ARD weights in FSL. Up to three fibers are shown for each voxel (fanning estimates not displayed).

vectors were used to estimate bingham distributions to generate orientation information for histology fibers, which were compared to the diffusion MRI predictions [4].

There again seems to generally be good agreement between histology and diffusion MRI predictions. A qualitative inspection of one of the crowns shown earlier in the image acquisition discussion suggests only minor differences in fiber orientation.

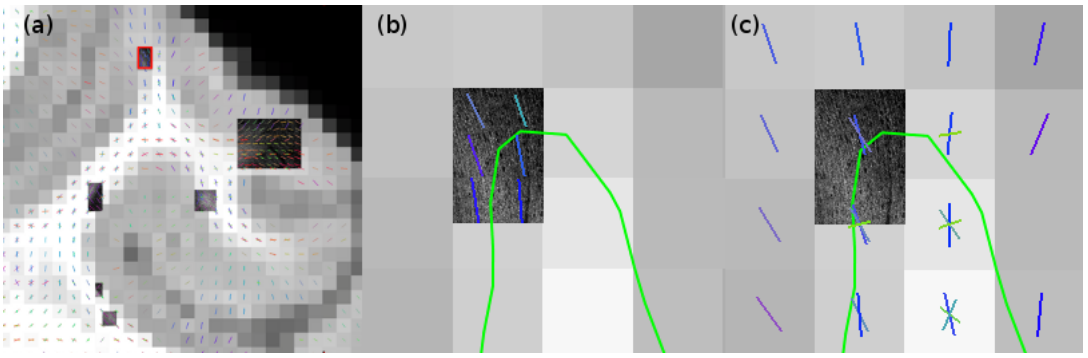

FIGURE 3.4: Comparison of histology and diffusion fibers at the crown of the supramarginal gyrus. (a) Location of a volume taken at the gyral crown (red box). (b) Histology fibers. (c) Diffusion fibers. Color-coding is used to show components oriented medial-lateral (red), dorso-ventral (blue), and antero-posterior (green). The gray/white boundary is delineated in green. Fibers at this crown seem in close agreement.

The major qualitative discrepancy to note is at the sulcal bank and the fundus, where diffusion MRI orientations that point towards cortex are much sparser. A series of figures compare results from the crown, bank, and sulcal fundus of the superior temporal gyrus.

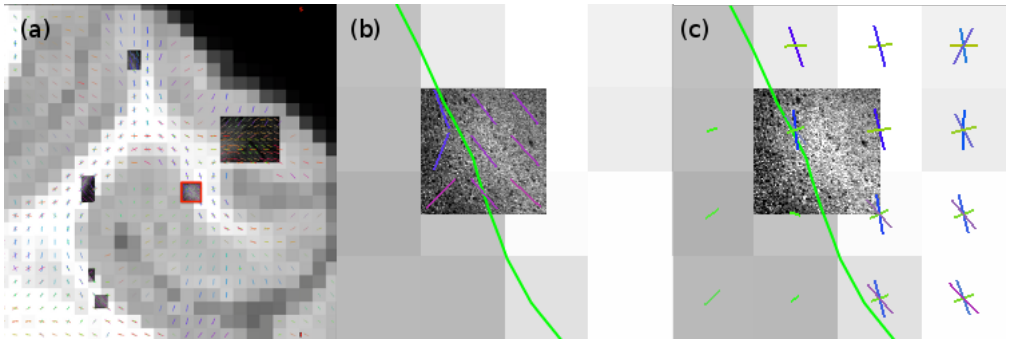

FIGURE 3.5: Comparison of histology and diffusion fibers near the crown of the superior temporal gyrus. (a) Location of a volume taken at the gyral crown (red box). (b) Histology fibers. (c) Diffusion fibers. Fiber orientations in both modalities seem able to model both the subcortical white matter fibers as well as fibers traversing the gray/white boundary, although the diffusion fibers seem to also be crossing the boundary with a significant antero-posterior component (green) whereas this is not as prominent in the histology.

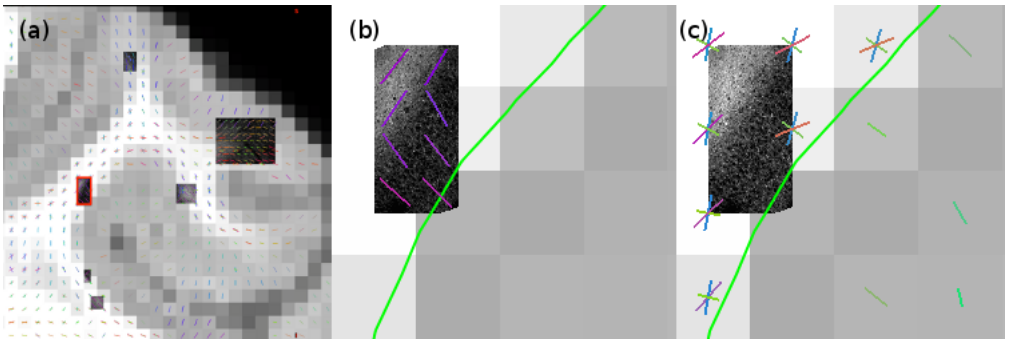

FIGURE 3.6: Comparison of histology and diffusion fibers at the sulcal bank of the superior temporal gyrus.(a) Location of a volume taken at the gyral bank (red box). (b) Histology fibers. (c) Diffusion fibers. Fiber orientations in both modalities seem able to model the subcortical white matter fibers. However, while the histology shows fibers crossing the gray/white boundary at a sharp angle, the diffusion shows only a few fibers taking sharp angles at the gray/white boundary. Compare this to the previous result which was closer to the gyral crown, where nearly all vertices along the white surface display some fiber angle that crosses the gray/white boundary.

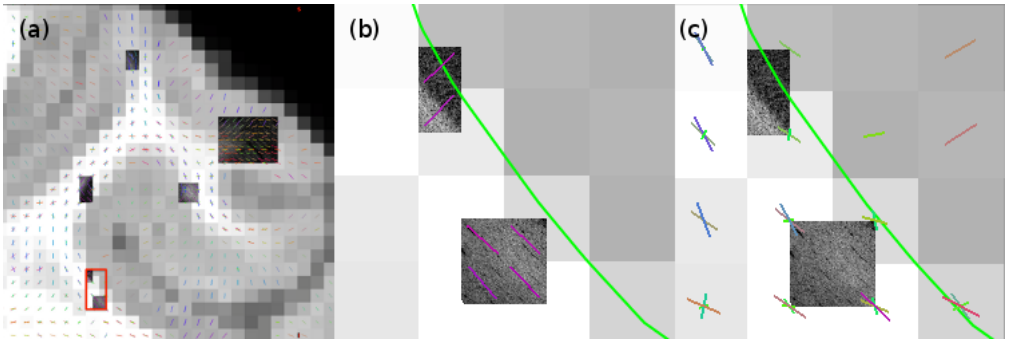

FIGURE 3.7: Comparison of histology and diffusion fibers at the sulcal fundus of the superior temporal gyrus.(a) Location of a volume taken at the sulcal fundus bank (red box). (b) Histology fibers. (c) Diffusion fibers. Fiber orientations in both modalities seem able to model the subcortical white matter fibers. However, the histology again shows fibers crossing the gray/white boundary at a sharp angle, where the diffusion shows very few fibers taking sharp angles at the gray/white boundary.

Histology and diffusion MRI are in good agreement in subcortical white matter in nearly all regions of the section. For fibers at the gray/white boundary, while diffusion estimates can often give similar orientations for axonal terminations as observed in the histology, these estimates are far fewer than what is expected when comparing with the histology. The weak signal from these radial fibers in the diffusion is likely one major component in preventing tractography streamlines from terminating more frequently along the sulcal banks and fundi.

3.4 Conclusion

With two-photon microscopy, it is now possible to generate three-dimensional fiber estimates from histology to compare with diffusion MRI estimates. From the data, subcortical white matter fibers in the diffusion MRI were in reasonable agreement the histology results, whereas fibers that cross the gray/white boundary and enter cortical gray matter show weak signal in the diffusion which is not present in the histology and is not likely to be an anatomically correct result. For future work, immediate improvements could potentially be made on the registration method, as the histology and MRI sections are imperfectly aligned in several regions. Furthermore, fiber estimates generated in the previous section can be used to produce quantitative comparisons of fiber direction. Ultimately, results from this comparison may inform diffusion modeling along the grey/white boundary.

Bibliography

[1] David C. Van Essen, Saad Jbabdi, Stamatios N. Sotiropoulos, Charles Chen, Krikor Dikranian, Tim Coalson, John Harwell, Timothy E.J. Behrens, and Matthew F. Glasser. Chapter 16 - Mapping Connections in Humans and Non-Human Primates: Aspirations and Challenges for Diffusion Imaging. In Heidi Johansen-Berg and Timothy E.J. Behrens, editors, *Diffusion MRI (Second Edition)*. Elsevier, 2014.

[2] N.T. Markov, M.M. Ercsey-Ravasz, A.R. Ribeiro Gomes, C. Lamy, L. Magrou, J. Vezoli, P. Misery, A. Falchier, R. Quilodran, M.A. Gariel, J. Sallet, R. Gamanut, C. Huissoud, S. Clavagnier, P. Giroud, D. Sappey-Marinier, P. Barone, C. Dehay, Z. Toroczkai, K. Knoblauch, D.C. Van Essen, and H. Kennedy. A weighted and directed interareal connectivity matrix for macaque cerebral cortex. *Cerebral Cortex*, 2012.

[3] H.E. D'Arceuil, S. Westmoreland, and A.J. de Crespigny. An approach to high resolution diffusion tensor imaging in fixed primate brain. *NeuroImage*, 2007.

[4] S.N. Sotiropoulos, T.E. Behrens, and S. Jbabdi. Ball and rackets: inferring fiber fanning from diffusion-weighted MRI. *NeuroImage*, 2012.

[5] T.E. Behrens, H.J. Berg, S. Jbabdi, M.F. Rushworth, and M.W. Woolrich. Probabilistic diffusion tractography with multiple fibre orientations: What can we gain? *NeuroImage*, 2007.

[6] M.D. Budde and J.A. Frank. Examining brain microstructure using structure tensor analysis of histological sections. *NeuroImage*, 2012.

[7] S.N. Sotiropoulos, C. Chen, K. Dikranian, S. Jbabdi, T.E. Behrens, D.C. Van Essen, and M.F. Glasser. Comparison of diffusion MRI predictions and histology in the Macaque brain. *Proceedings of the International Society for Magnetic Resonance in Medicine (ISMRM) Annual Meeting*, 2013.

[8] K. Chung, J. Wallace, S.Y. Kim, S. Kalyanasundaram, A.S. Andalman, T.J. Davidson, J.J. Mirzabekov, K.A. Zalocusky, J. Mattis, A.K. Denisin, S. Pak, H. Bernstein,

C. Ramakrishnan, L. Grosenick, V. Gradinaru, and K. Deisseroth. Structural and molecular interrogation of intact biological systems. *Nature*, 2013.